

On Splitting-Based Numerical Methods for Convection-Diffusion Equations

Alina Chertock[†] and Alexander Kurganov[‡]

Abstract

Convection-diffusion equations model a variety of physical phenomena. Computing solutions of these equations is an important and challenging problem, especially in the convection dominated case, in which viscous layers are so thin that one is forced to use underresolved methods that may be unstable. If an insufficient amount of physical diffusion is compensated by an excessive numerical viscosity, the underresolved method is typically stable, but the resolution may be severely affected. At the same time, the use of dispersive schemes may cause spurious oscillations that may, in turn, trigger numerical instabilities. In this paper, we review a special operator splitting technique that may help to overcome these difficulties by numerically preserving a delicate balance between the convection and diffusion terms, which is absolutely necessary when an underresolved method is used. We illustrate the performance of the splitting-based methods on a number of numerical examples including the polymer system arising in modeling of the flooding processes in enhanced oil recovery, systems modeling the propagation of a passive pollutant in shallow water, and the incompressible Navier-Stokes equations.

1 Introduction

This paper is focused on numerical methods for (systems of) convection-diffusion equations that arise in a variety of applications and represent mathematical models for a number of (physical) processes in fluid mechanics, astrophysics, meteorology, multiphase flow in oil reservoirs, polymer flow, financial modeling, and many other areas.

We consider the initial value problem (IVP)

$$\mathbf{q}_t + \nabla_{\mathbf{x}} \cdot \mathbf{f}(\mathbf{q}) = D\Delta\mathbf{q}, \quad \mathbf{q}(\mathbf{x}, 0) = \mathbf{q}_0(\mathbf{x}), \quad (1.1)$$

where, $\mathbf{q}(\mathbf{x}, t) = (q_1(\mathbf{x}, t), \dots, q_l(\mathbf{x}, t))^T$ is an unknown l -vector, \mathbf{f} is a nonlinear convection flux, and $D = \text{diag}(\varepsilon_1, \dots, \varepsilon_l)$ is a constant diagonal matrix with positive entries. In the general multidimensional case, \mathbf{q} is a vector function of a time variable t and d -dimensional spatial variable $\mathbf{x} = (x_1, \dots, x_d)$ with corresponding fluxes $\mathbf{f} = (f^1, \dots, f^d)$. We also consider a closely related viscous Hamilton-Jacobi (HJ) equation

$$\varphi_t + H(\varphi_{x_1}, \dots, \varphi_{x_d}) = \varepsilon\Delta\varphi, \quad (1.2)$$

[†]Department of Mathematics, North Carolina State University, Raleigh, NC 27695; chertock@math.ncsu.edu

[‡]Mathematics Department, Tulane University, New Orleans, LA 70118; kurganov@math.tulane.edu

where $\varphi(\mathbf{x}, t)$ is an unknown function, H is a nonlinear Hamiltonian, and ε is a positive constant.

It is well-known that the considered models are parabolic and thus they admit global smooth solutions even for discontinuous initial data. This makes it easy to design stable and convergent numerical methods for (1.1). Their resolution, however, will depend on the size of the diffusion coefficients as illustrated in the following simple example, in which we consider the scalar one-dimensional (1-D) version of (1.1):

$$q_t + f(q)_x = \varepsilon q_{xx}. \quad (1.3)$$

A standard second-order central difference discretization of the spatial derivatives in (1.3) results in the following semi-discrete finite-difference (FD) scheme:

$$\frac{dq_j}{dt} = -\frac{f(q_{j+1}) - f(q_{j-1}))}{2\Delta x} + \varepsilon \frac{q_{j+1} - 2q_j + q_{j-1}}{(\Delta x)^2}. \quad (1.4)$$

Here, Δx is the size of the spatial grid, which is, for simplicity, assumed to be uniform, and $q_j \equiv q_j(t)$ is the semi-discrete approximation of $q(x_j, t)$ at the grid point x_j . When Δx is small the ODE system (1.4) is stiff and thus should be integrated by a stable and sufficiently accurate ODE solver (see, e.g., [3, 23, 26]).

Even though the resulting fully-discrete method is stable and convergent as $\Delta x \rightarrow 0$, its performance on a fixed grid heavily depends on the ratio between Δx and ε . This can be clearly seen in Figure 1.1, where we plot the solutions of (1.3) with $\varepsilon = 2.5 \cdot 10^{-1}$ and $5 \cdot 10^{-3}$, computed by the FD scheme (1.4) on a coarse ($\Delta x = 4 \cdot 10^{-2}$) and a fine ($\Delta x = 1.25 \cdot 10^{-3}$) uniform grids. As one can observe, the coarse grid solution is acceptable in the case of the larger $\varepsilon = 2.5 \cdot 10^{-1}$ only. This is due to the fact that the width of the viscous shock layer is proportional to ε and therefore, the layer cannot be resolved when $\Delta x \gg \varepsilon$. In order to obtain a highly resolved numerical solution in the case of the smaller $\varepsilon = 5 \cdot 10^{-3}$, one has to significantly refine the grid (see Figure 1.1(c)).

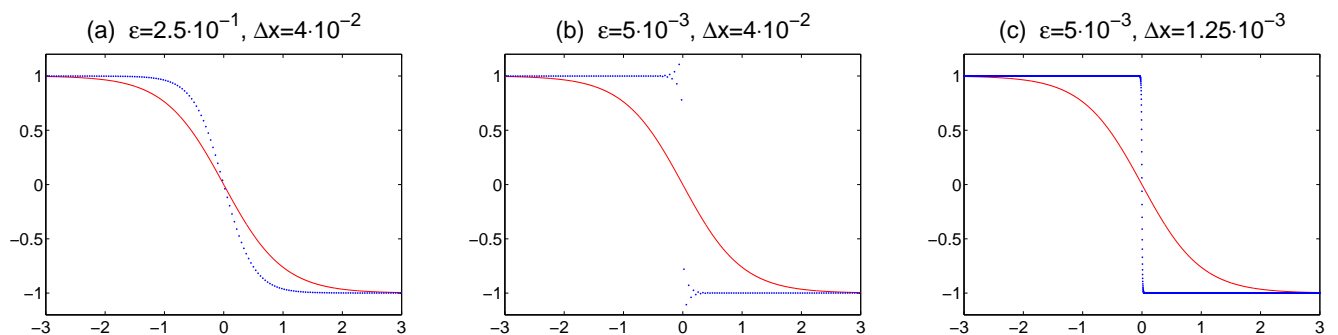


Figure 1.1: Steady-state solutions of (1.3) with $f(q) = q^2/2$ and $\varepsilon = 5 \cdot 10^{-1}$ (a) and $\varepsilon = 5 \cdot 10^{-3}$ (b,c) computed on coarse (a,b) and fine (c) grids. The solid line represents the initial data $q(x, 0) = \tanh x$.

This simple example demonstrates that the convection dominated regime ($\varepsilon \ll 1$) is the most challenging one from a numerical perspective since utilizing the grid refinement strategy for small ε may be computationally unaffordable, especially in the multidimensional case. In practice, one is forced to use underresolved methods (with $\Delta x \gg \varepsilon$) and therefore may want to ignore the right-hand side (RHS) of (1.1) by taking $\varepsilon_i = 0 \forall i$, and applying a shock-capturing method to the

resulting hyperbolic system, see, e.g., [17, 20, 30, 38, 39]. This, however, may produce unphysical shocks and boundary layers solely determined by numerical diffusion.

One way to overcome this difficulty is to use an operator splitting method, which can be briefly described as follows. Consider the system (1.1) and denote by $\mathcal{S}_{\mathcal{H}}$ the *exact* solution operator associated with the corresponding hyperbolic system:

$$\mathbf{q}_t + \nabla_{\mathbf{x}} \cdot \mathbf{f}(\mathbf{q}) = 0, \quad (1.5)$$

and by $\mathcal{S}_{\mathcal{P}}$ the *exact* solution operator associated with the (linear) parabolic system

$$\mathbf{q}_t = D\Delta\mathbf{q}. \quad (1.6)$$

Let us assume that the solution of the original convection-diffusion system (1.1) is available at time t . We then introduce a (small) time step Δt and evolve the solution of (1.1) from t to $t + \Delta t$ in two substeps. First, the hyperbolic system (1.5) is solved on the time interval $(t, t + \Delta t]$:

$$\mathbf{q}^*(\mathbf{x}) = \mathcal{S}_{\mathcal{H}}(\Delta t)\mathbf{q}(\mathbf{x}, t), \quad (1.7)$$

and then the parabolic solution operator is applied to \mathbf{q}^* , which results in the following approximate solution at time $t + \Delta t$:

$$\mathbf{q}(\mathbf{x}, t + \Delta t) = \mathcal{S}_{\mathcal{P}}(\Delta t)\mathbf{q}^*(\mathbf{x}) = \mathcal{S}_{\mathcal{P}}(\Delta t)\mathcal{S}_{\mathcal{H}}(\Delta t)\mathbf{q}(\mathbf{x}, t). \quad (1.8)$$

In general, if all solutions involved in the two-step splitting algorithm (1.7)–(1.8) are smooth, the operator splitting method is *first-order* accurate (see, e.g., [41, 42, 51]).

Higher-order operator splitting algorithms can be derived by considering additional substeps. For instance, one time step of the *second-order* Strang splitting method [41, 42, 51] consists of three substeps:

$$\mathbf{q}(\mathbf{x}, t + \Delta t) = \mathcal{S}_{\mathcal{H}}(\Delta t/2)\mathcal{S}_{\mathcal{P}}(\Delta t)\mathcal{S}_{\mathcal{H}}(\Delta t/2)\mathbf{q}(\mathbf{x}, t). \quad (1.9)$$

All splitting algorithms, presented in this paper, are based on the Strang splitting algorithm (1.9). We also refer the reader to [56], where similar splitting methods were derived by simply choosing certain longer time increment sequences, while again alternating $\mathcal{S}_{\mathcal{H}}$ and $\mathcal{S}_{\mathcal{P}}$. The time increments of methods of orders 4, 6 and 8 can be found, for example, in [37]. Although they are, in general, not unique, it can be shown that splitting methods of orders higher than two will require some negative time increments [52], which may cause numerical instability when time irreversible (dissipative) systems are solved.

In practice, the exact solution operators $\mathcal{S}_{\mathcal{H}}$ and $\mathcal{S}_{\mathcal{P}}$ are to be replaced by their numerical approximations. Note that the hyperbolic, (1.5), and the parabolic, (1.6), subproblems, which are of different nature, can be solved by different numerical methods — this is one of the main advantages of the operator splitting technique.

Hyperbolic Solvers. The choice of a discrete hyperbolic solution operator is typically motivated by the properties of the flux function in (1.5) or the Hamiltonian in (1.2). If $\mathbf{f}(\mathbf{q})$ is nonlinear, then (1.5) is a hyperbolic system of conservation laws, whose solutions are generically discontinuous. In this case, the system (1.5) should be solved by a shock-capturing scheme, see, e.g., [17, 20, 30, 38]. If H is nonlinear, the corresponding inviscid HJ equation should be solved by an appropriate high-resolution method, see e.g., [7, 8, 27, 32, 45, 46, 49, 55]. If $\mathbf{f}(H)$ is linear, then the shock-capturing techniques may be overly diffusive, so that one may prefer to use either a spectral (see, e.g. [21, 25, 50]) method, a particle method (see, e.g. [16, 18, 47]), or the method of characteristics.

Parabolic Solvers. Using the method of lines, the parabolic subproblem (1.6) can be reduced to a system of ODEs, which can be efficiently and accurately integrated by an appropriate implicit (see, e.g., [3, 23]), large stability domains explicit [1, 2, 26, 43], or implicit-explicit (see, e.g., [3, 4]) ODE solver. As an alternative, (1.6) may be solved exactly using the heat kernel solution formula, as proposed in [11, 13, 14], or using a pseudo-spectral method. In the latter cases, there is no stability restriction on the size of the “parabolic” substep, which is the key point in designing an efficient explicit method.

In this paper, we provide a detailed description of three different versions of a **fast explicit operator splitting method**:

- *Version I* (see §2): **FV-GF method**, which is based on the finite-volume (FV) hyperbolic solver and the exact parabolic solver implemented by discretizing the convolution with the Green function formula for the exact solution of the heat equation;
- *Version II* (see §3): **MC-GF method**, in which the hyperbolic solver is the method of characteristics (MC) while the parabolic solver is the same as in the FV-GF method;
- *Version III* (see §4): **FD-PS method**, which is based on a high-order FD scheme and the exact parabolic solver implemented in the pseudo-spectral manner.

We note that the FV-GF and the MC-GF methods have been recently proposed in [13, 14] and [11], respectively, while the FD-PS method is new.

Depending on the convection-diffusion model at hand, one of the above versions may be particularly advantageous. In §2, we consider the system (1.1) with a nonlinear flux function \mathbf{f} , for which the FV-GF method seems to be a natural choice since its hyperbolic solver is designed to treat (systems of) hyperbolic conservation laws. Our particular choice of the FV method is the second-order Godunov-type central-upwind schemes [31, 32, 35]. In §2.2, the resulting method is applied to the Burgers equation and to a polymer system modeling flooding processes in enhanced oil recovery, [28, 48, 54].

The MC-GF method, on the other hand, seems to be optimal when the hyperbolic problem is linear and thus can be easily solved by the method of characteristics, which is diffusion-free. The latter guarantees that the only diffusion present in the splitting method is the physical one because it comes from the parabolic part. In §3.1, the MC-GF method is applied to a linear convection-diffusion equation as well as to a model describing the propagation of a passive pollutant in shallow water.

Finally, the FD-PS method seems to be preferable in the case of a viscous HJ equation with periodic boundary conditions, in which one may take advantage of the FFT algorithm to significantly speed up the implementation of the exact parabolic solver. In §4, we apply the FD-PS method to the vorticity formulation of the two-dimensional (2-D) incompressible Navier-Stokes (NS) equations written in the transport form and thus can be viewed as a HJ equation with a global Hamiltonian. Our particular choice for the hyperbolic solver is a fourth-order FD scheme based on the central-upwind numerical Hamiltonian from [32] and the fifth-order Weighted Power-ENO reconstruction [10, 49].

2 The FV-GF Method

In this section, we describe the first version of the fast explicit operator splitting method — the FV-GF method — in which we combine a FV hyperbolic solver and a Green function based parabolic solver (this is the original fast explicit operator splitting method proposed in [13, 14]). For simplicity, we present only its one-dimensional (1-D) version. The 2-D version can be found in [13].

The FV-GF method is based on the Strang operator splitting (1.9) applied to the system (1.1). The “hyperbolic” substep is carried out using a Godunov-type FV scheme, in which a piecewise polynomial interpolant is first reconstructed from cell averages (computed at the previous time step), and then evolved to the next time level according to the integral form of the hyperbolic system (1.5). More precisely, the projection-evolution Godunov-type approach may be described as follows.

Assume that we have computed the cell averages of the solution over a uniform grid (the extension to nonuniform Cartesian grids is pretty straightforward) at some time level t :

$$\bar{\mathbf{q}}_j(t) \approx \bar{\mathbf{q}}(x_j, t) := \frac{1}{\Delta x} \int_{I_j} \mathbf{q}(x, t) dx, \quad I_j := (x_{j-\frac{1}{2}}, x_{j+\frac{1}{2}}).$$

We then reconstruct a piecewise polynomial interpolant for each component of the vector $\mathbf{q} = (q_1, \dots, q_l)^T$. The (formal) order of accuracy of these reconstructions usually determines the (formal) spatial order of the resulting FV scheme. In this paper, we will focus on second-order schemes that require conservative piecewise linear reconstructions of the following form:

$$\tilde{\mathbf{q}}(x; t) = \bar{\mathbf{q}}_j(t) + \mathbf{q}'_j(x - x_j) \quad \text{for } x \in I_j, \quad (2.1)$$

where the slopes \mathbf{q}'_j have to be (at least) first-order component-wise approximations of the partial derivatives $\mathbf{q}_x(x_j, t)$. In order to ensure a non-oscillatory behavior of the reconstruction, which is a necessary condition for the overall scheme to be non-oscillatory, the slopes should be computed with the help of a nonlinear limiter. In the reported numerical experiments, we have used the one-parameter family of *minmod* limiters (see, e.g., [40, 44, 53]), applied in a component-wise manner:

$$\mathbf{q}'_j = \text{minmod} \left(\theta \frac{\bar{\mathbf{q}}_{j+1}(t) - \bar{\mathbf{q}}_j(t)}{\Delta x}, \frac{\bar{\mathbf{q}}_{j+1}(t) - \bar{\mathbf{q}}_{j-1}(t)}{2\Delta x}, \theta \frac{\bar{\mathbf{q}}_j(t) - \bar{\mathbf{q}}_{j-1}(t)}{\Delta x} \right), \quad (2.2)$$

where $\theta \in [1, 2]$, and the multivariate *minmod* function is defined by

$$\text{minmod}(z_1, z_2, \dots) := \begin{cases} \min_j \{z_j\}, & \text{if } z_j > 0 \quad \forall j, \\ \max_j \{z_j\}, & \text{if } z_j < 0 \quad \forall j, \\ 0, & \text{otherwise.} \end{cases}$$

Notice that larger θ 's correspond to less dissipative but, in general, more oscillatory limiters.

The solution at the new time level $t + \Delta t_{\text{HYP}}$ is then obtained by evolving the piecewise linear interpolant (2.1) in time according to the integral form of the system (1.5), obtained by

integrating it over the control volume $I_j \times [t, t + \Delta t_{\text{HYP}}]$:

$$\bar{\mathbf{q}}(x_i, t + \Delta t_{\text{HYP}}) = \bar{\mathbf{q}}(x_i, t) - \frac{1}{\Delta x} \int_t^{t+\Delta t_{\text{HYP}}} \left\{ \mathbf{f}(\mathbf{q}(x_{j+\frac{1}{2}}, \tau)) - \mathbf{f}(\mathbf{q}(x_{j-\frac{1}{2}}, \tau)) \right\} d\tau. \quad (2.3)$$

This may be done using any FV evolution approach. In this paper, we have used the semi-discrete central-upwind scheme from [32], see also [31, 35]. We note, however, that the ‘‘hyperbolic’’ substep of the FV-GF method is not tied up to a specific choice of a FV scheme and can be implemented with any Godunov-type method.

Remark 2.1 Note that due to the CFL condition, Δt_{HYP} may be smaller than $\Delta t/2$, where Δt is the size of the splitting step. In this case, the approximate ‘‘hyperbolic’’ substep of the splitting algorithm would consist of several smaller ‘‘FV subsubsteps’’ of size Δt_{HYP} . This is a typical situation, for example, in applications to polymer flows (see §2.2), where one is interested in developing a reliable operator splitting method that is capable to produce a high quality approximate solution with a small number of splitting steps, that is, while keeping Δt relatively large (see, e.g., [29] and the references therein). ■

Once the solution of the first ‘‘hyperbolic’’ substep in (1.9) is performed, the intermediate cell averages

$$\bar{\mathbf{q}}_j^* \approx \frac{1}{\Delta x} \int_{I_j} \mathcal{S}_{\mathcal{H}}(\Delta t/2) \mathbf{q}(x, t) dx$$

become available, and we reconstruct another piecewise linear interpolant $\tilde{\mathbf{q}}^*(x)$ following (2.1)–(2.2). This piecewise linear function is then used as an initial condition for the parabolic IVP:

$$\mathbf{q}_t = D\mathbf{q}_{xx}, \quad \mathbf{q}(x, t) = \tilde{\mathbf{q}}^*(x), \quad (2.4)$$

which is now, according to the Strang splitting algorithm (1.9), to be solved on the time interval $(t, t + \Delta t]$.

Note that since D is a diagonal matrix, the parabolic system in (2.4) is actually a set of l uncoupled heat equations for each component of \mathbf{q} :

$$(q_i)_t = \varepsilon_i (q_i)_{xx}, \quad q_i(x, t) = \tilde{q}_i^*(x), \quad i = 1, \dots, l. \quad (2.5)$$

From now on, we will simplify our notation by using q instead of any of the q_i ’s and ε instead of any of the ε_i ’s.

Next, we recall that in the 1-D case, the exact solution of (2.5) at time $t + \Delta t$ may be expressed in the following integral form:

$$q^{**}(x) := q(x, t + \Delta t) = \int_{\mathbb{R}} G(x - \xi, \varepsilon \Delta t) \tilde{q}^*(\xi) d\xi, \quad (2.6)$$

where G is the heat kernel:

$$G(x, t) = \frac{1}{\sqrt{4\pi t}} e^{-\frac{x^2}{4t}}. \quad (2.7)$$

Notice that for small $\varepsilon\Delta t$ the expression $G(x - \xi, \varepsilon\Delta t)$ is almost singular at $x \sim \xi$ and hence formula (2.6) may be impractical. Therefore we use the fact that

$$\int_{\mathbb{R}} G(x - \xi, \varepsilon\Delta t) d\xi = 1$$

and rewrite (2.6) in the equivalent symmetric form:

$$q^{**}(x) = \tilde{q}^*(x) + \int_{\mathbb{R}} G(x - \xi, \varepsilon\Delta t) (\tilde{q}^*(\xi) - \tilde{q}^*(x)) d\xi. \quad (2.8)$$

This allows one to remove the singularity from the original formula and at the same time to preserve the conservation of q , that is, to ensure that the equality

$$\int_{\mathbb{R}} q^{**}(x) dx = \int_{\mathbb{R}} \tilde{q}^*(x) dx$$

is satisfied on the discrete level as well.

Since for the next “hyperbolic” substep only the cell averages of $q^{**}(x)$ are needed, we average (2.8) over the corresponding computational cells to obtain:

$$\begin{aligned} \bar{q}_j^{**} &= \bar{q}_j^* + \frac{1}{\Delta x} \int_{I_j} \left[\int_{\mathbb{R}} G(x - \xi, \varepsilon\Delta t) (\tilde{q}^*(\xi) - \tilde{q}^*(x)) d\xi \right] dx \\ &= \bar{q}_j^* + \frac{1}{\Delta x} \sum_{i \in \mathbb{Z}} \int_{I_j} \int_{I_i} G(x - \xi, \varepsilon\Delta t) (\tilde{q}^*(\xi) - \tilde{q}^*(x)) d\xi dx. \end{aligned} \quad (2.9)$$

Next, the integrals on the RHS of (2.9) are discretized using the midpoint quadrature, that is,

$$\bar{q}_j^{**} = \bar{q}_j^* + \Delta x \sum_{i \in \mathbb{Z}} G(x_j - x_i, \varepsilon\Delta t) (\bar{q}_i^* - \bar{q}_j^*). \quad (2.10)$$

Remark 2.2 In practice, the computational domain is finite and the infinite sum on the RHS of (2.10) reduces to the sum over all computational cells (we obviously need to assume that the solution decreases exponentially fast near the artificially imposed boundaries). ■

Remark 2.3 The midpoint quadrature (2.10) is conservative:

$$\sum_{j \in \mathbb{Z}} \bar{q}_j^{**} = \sum_{j \in \mathbb{Z}} \bar{q}_j^* + \Delta x \sum_{j, i \in \mathbb{Z}} G(x_j - x_i, \varepsilon\Delta t) (\bar{q}_i^* - \bar{q}_j^*) = \sum_{j \in \mathbb{Z}} \bar{q}_j^*,$$

since $G(\pm(x_j - x_i), \varepsilon\Delta t) = G(x_j - x_i, \varepsilon\Delta t)$ due to the symmetry of the heat kernel (2.7). We also note that one may use a higher-order quadrature for discretizing the integrals in (2.9), which will be conservative as long as the quadrature is symmetric. ■

The third and last substep of the FV-GF method is again “hyperbolic”. We start with the cell averages $\bar{\mathbf{q}}_j^{**}$, computed at the “parabolic” substep, reconstruct a piecewise linear interpolant $\hat{\mathbf{q}}$ (following (2.1)–(2.2)), and then evolve it using the same FV scheme (2.3) as in the first “hyperbolic” substep to obtain the cell averages of the solution of (1.1) at the new time level $t + \Delta t$,

$$\bar{\mathbf{q}}_j(t + \Delta t) \approx \frac{1}{\Delta x} \int_{I_j} \mathcal{S}_{\mathcal{H}}(\Delta t/2) \hat{\mathbf{q}}(x) dx.$$

This completes the description of one time step of the FV-GF method.

2.1 Convergence Results — An Overview

The convergence rate of the FV-GF method has been extensively studied in [13]. Here, we briefly summarize the 1-D error analysis presented in [13, §2.1].

At each splitting step ($t \rightarrow t + \Delta t$), the L^∞ -error of the studied method, $E(\Delta t)$, is a sum of three errors: the operator splitting error $E_S(\Delta t)$, the error $E_{\mathcal{H}}(\Delta t)$ of the “hyperbolic” substep and the error $E_{\mathcal{P}}(\Delta t)$ of the “parabolic” substep. The latter error is the quadrature error, whose bounds are established in the following theorem (notice that the resulting bounds depend on the smoothness of the solution).

Theorem 2.1 *Let \tilde{q}^* be a (formally) second-order piecewise linear approximation of the piecewise smooth function q^* ,*

$$\tilde{q}^*(x) = \bar{q}_j^* + q_j'(x - x_j) \quad \text{for } x \in I_j,$$

where \bar{q}_j^* is a computed cell average of q^* over the interval I_j and q_j' is (at least) a first-order approximation of $q_x^*(x_j)$. Assume that $|\tilde{q}^*(x)| \leq C$ for all $x \in \mathbb{R}$ and $|q_j'| \leq C(\Delta x)^{-1}$ for all j . Then the error $E_{\mathcal{P}}(\Delta t)$ of the “parabolic” substep in the FV-GF method can be bounded by

$$E_{\mathcal{P}}(\Delta t) \leq C \left(\frac{\Delta x}{\sqrt{\varepsilon \Delta t}} \right), \quad \text{provided } \frac{\Delta x}{\sqrt{\varepsilon \Delta t}} \leq 1, \quad (2.11)$$

where C is an absolute constant that is independent of Δt , Δx , and $\varepsilon := \max(\varepsilon_1, \dots, \varepsilon_l)$.

If, in addition, we assume that q^* is smooth, in particular, $q^* \in C^2(\mathbb{R})$ and $|q_{xx}^*(x)| \leq C$ for all $x \in \mathbb{R}$, then a sharper bound can be obtained:

$$E_{\mathcal{P}}(\Delta t) \leq C_1(\Delta x)^2 + C_2 \frac{(\Delta x)^4}{(\varepsilon \Delta t)^2} + C_3 \frac{(\Delta x)^4}{(\varepsilon \Delta t)^{3/2}}, \quad (2.12)$$

where C, C_1, C_2 , and C_3 are absolute constants that are independent of $\Delta t, \Delta x$, and ε .

The splitting, $E_S(\Delta t)$, and the “hyperbolic”, $E_{\mathcal{H}}(\Delta t)$, errors are hard (if not impossible) to estimate in the case of a nonlinear flux \mathbf{f} since then the solution of the hyperbolic subproblem may develop discontinuities. However, if the flux function is linear and the initial data are smooth, the solutions of both (1.5) and (1.6) preserve their initial smoothness, and $E_S(\Delta t)$ and $E_{\mathcal{H}}(\Delta t)$ can be bounded at each time step as follows:

$$E_S(\Delta t) \leq C(\varepsilon \Delta t)^3, \quad E_{\mathcal{H}}(\Delta t) \leq C \Delta t (\Delta x)^2. \quad (2.13)$$

The latter estimate is obtained assuming that the hyperbolic subproblem has been numerically solved using a convergent, uniformly second-order method.

Now, adding the three components of the error, given by (2.12) and (2.13), at each time step and taking into account that the total number of splitting steps is proportional to $1/\Delta t$, one ends up with the following estimate for the global L^∞ -error in the case of a linear flux and smooth initial data:

$$E(\Delta t) \leq C \left[\varepsilon^3 (\Delta t)^2 + (\Delta x)^2 + \frac{(\Delta x)^2}{\Delta t} + \frac{(\Delta x)^4}{\Delta t (\varepsilon \Delta t)^2} + \frac{(\Delta x)^4}{\Delta t (\varepsilon \Delta t)^{3/2}} \right]. \quad (2.14)$$

Notice that the presence of the ε^3 factor in the first term on the RHS of (2.14), ensures that even when the size of the splitting step Δt is large, the overall error may be small in the convection-dominated case, that is, when ε is small. This allows one to achieve a very high resolution with only few splitting steps and thus to increase the efficiency of the operator splitting method.

Remark 2.4 We would like to emphasize that errors in (2.11), (2.12), and (2.14) are proportional to $(\Delta t)^\alpha$ with $\alpha < 0$. Therefore, the size of splitting steps should not be taken too small as we illustrate in Example 2.2 (see Tables 2.1–2.3). ■

2.2 Numerical Examples

In this section, we demonstrate the performance of the FV-GF method on a number of test problems. In all the examples, the “hyperbolic” substep was performed using the second-order central-upwind scheme from [32].

Example 2.1 — Burgers’ Equation

We apply the FV-GF method to the IVP

$$q_t + \left(\frac{q^2}{2} \right)_x = \varepsilon q_{xx}, \quad q(x, 0) = -\tanh x \quad (2.15)$$

with $\varepsilon = 0.005$ (notice that this is the same IVP, which has been considered in the introduction). The computational domain is $[-4, 4]$, and the final time is $t = 4$, by which the solution practically converges to the steady state. The hyperbolic solver employs the minmod limiter (2.2) with $\theta = 2$.

The computed solutions of (2.15) together with the exact one, given by the Hopf formula,

$$q(x, t) = \frac{\int_{-\infty}^{\infty} (x - \xi) e^{-\frac{\lambda(x, \xi, t)}{2\varepsilon}} d\xi}{\int_{-\infty}^{\infty} t e^{-\frac{\lambda(x, \xi, t)}{2\varepsilon}} d\xi}, \quad \lambda(x, \xi, t) := \frac{(x - \xi)^2}{2t} + \int_0^\xi q(\eta, 0) d\eta,$$

are shown in Figures 2.1–2.3. In Figure 2.1, we show the results obtained on a coarse grid with $\Delta x = 4 \cdot 10^{-2} \gg \varepsilon = 5 \cdot 10^{-3}$. First, we compute the solution using the FV-GF method with 2 splitting steps only, which corresponds to a very large splitting stepsize $\Delta t = 2$, see Figure 2.1(a). We then apply the FV-GF method with 128 splitting steps (that is, we take a much smaller splitting stepsize $\Delta t = 3.125 \cdot 10^{-2}$) and obtain a very similar result plotted in Figure 2.1(b). As one can observe, the quality of the underresolved results are very high, independently

of the number of splitting steps (compare with the FD solution in Figure 1.1(b)). Obviously, the shock layer cannot be resolved on such a coarse grid. We therefore refine the grid to $\Delta x = 0.01$, which leads to a better resolution of the shock layer. The results obtained with 16, 32, 64, and 128 splitting steps are shown in Figures 2.2(a), (b), (c), and (d), respectively. As one can clearly see there, the quality of the computed solution now depends on the number of splitting steps. However, in this calculation Δx is still larger than ε , so one still cannot fully resolve the shock layer yet. We then further refine the grid and take $\Delta x = 1.25 \cdot 10^{-3} < \varepsilon = 5 \cdot 10^{-3}$ (the same fine grid has been used to compute the FD solution shown in Figure 1.1(c)). The dependence of the quality of the obtained results on the number of splitting steps is even more pronounced now, as one can see in Figure 2.3. We stress that the shock layer can be fully resolved with 128 splitting steps, which corresponds to $\Delta t = 3.125 \cdot 10^{-2} \gg \Delta x = 1.25 \cdot 10^{-3}$. This demonstrates a high efficiency of the FV-GF method.

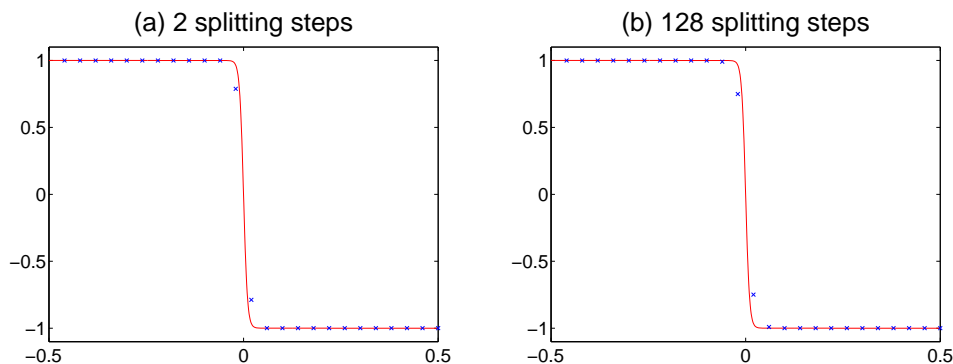


Figure 2.1: Numerical solutions of (2.15) computed with $\Delta x = 4 \cdot 10^{-2}$ and different numbers of splitting steps vs. the exact solution (solid line).

Example 2.2 — Polymer System

In this section, we apply the FV-GF method to a 1-D model describing flow in porous media. We numerically solve the system of convection-diffusion equations

$$\begin{cases} s_t + p(s, c)_x = \varepsilon s_{xx}, \\ w_t + (c p(s, c))_x = \varepsilon w_{xx}, \end{cases} \quad w = w(s, c) = s c + e(c), \quad (2.16)$$

subject to the initial data

$$(s, c)(x, 0) = \begin{cases} (0.75, 0.8), & x \leq 0.25, \\ (0.839619, 0.4), & x > 0.25. \end{cases} \quad (2.17)$$

Here, s is the water saturation, c is the polymer concentration in the water, $\varepsilon = 0.005$ is a small scaling parameter, and

$$p(s, c) = \frac{s^2}{s^2 + (c + 0.5)(1 - s)^2} \quad \text{and} \quad e(c) = \frac{c}{5(1 + c)}$$

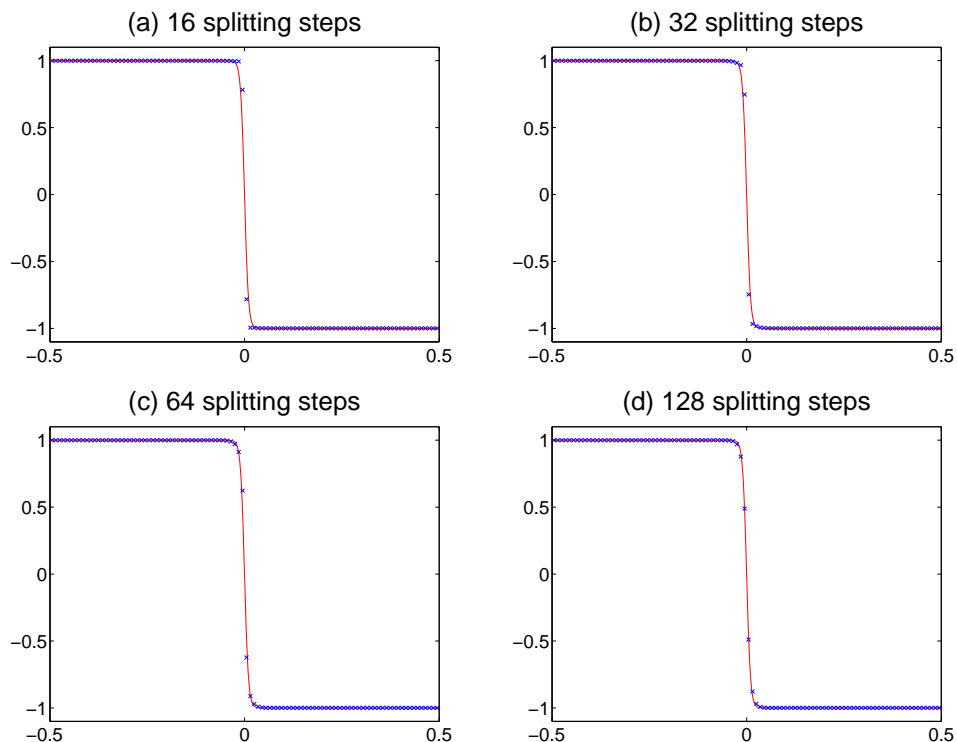


Figure 2.2: Numerical solutions of (2.15) computed with $\Delta x = 10^{-2}$ and different numbers of splitting steps vs. the exact solution (solid line).

are the fractional flow and absorption functions, respectively.

This system models polymer flooding processes in enhanced oil recovery (see [28, 48, 54] and references therein). The initial data, taken from [29] and [24], corresponds to a Riemann problem whose solution in the inviscid case contains a compressive shock, in which both the s - and the c -characteristics go into the shock and contribute to its self-sharpening. If this Riemann problem is slightly perturbed, the solution changes from a single shock to a composition of waves moving with almost the same speed (see, e.g., [29]). There are two possible results of the perturbation: either a monotone or a nonmonotone solution. In the viscous case, the problem will be perturbed instantly, which results in a truly nonlinear phenomenon: monotone initial data evolve into nonmonotone solutions.

We compare the numerical solution computed by the FV-GF method with a reference solution obtained without any operator splitting by combining the second-order central-upwind scheme with the explicit second-order central difference approximation for the diffusion term in (2.16). In all calculations, we take the value of the minmod (see (2.2)) parameter $\theta = 1$, since the flux here is nonconvex and, as it has been demonstrated in [34], the use of a compressive minmod limiter with $\theta > 1$ may lead to a convergence to a “wrong” solution that does not satisfy the entropy condition for all entropies. Obviously, this will not be a problem when ε is large, but we are focusing on the convection-dominated regime, in which a large error at the “hyperbolic” substep cannot be “fixed” by a small diffusion acting at the “parabolic” substep.

In Figure 2.4, we plot the approximate solutions of (2.16)–(2.17) (dotted lines) at time $t = 1$, computed by the FV-GF method with two and four splittings steps. We compare the solutions

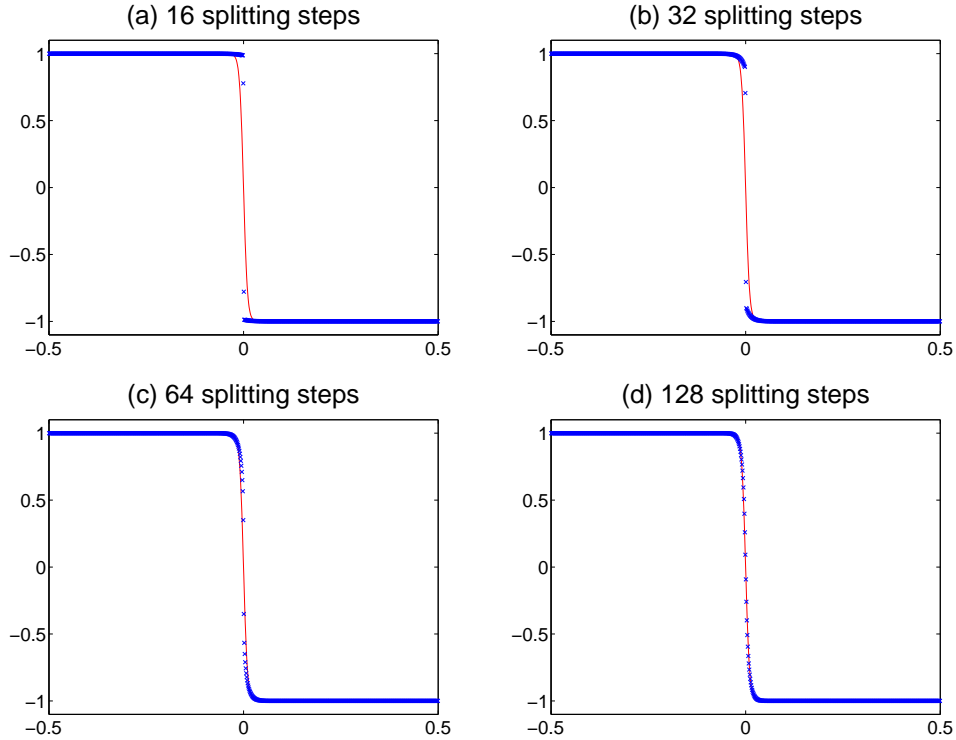


Figure 2.3: Numerical solutions of (2.15) computed with $\Delta x = 1.25 \cdot 10^{-3}$ and different numbers of splitting steps vs. the exact solution (solid line).

computed with 500 uniform grid cells with the corresponding reference solutions computed with 10000 cells. The s -component of the exact (reference) solution has a dip due to the presence of the diffusion term. As one can observe, this dip is not well-resolved when only 2 or 4 splitting steps are performed. Therefore, we apply the FV-GF method with 8 and 32 splittings steps and show the obtained results in Figure 2.5. As one can see there, a very high resolution is achieved. We would like to point out that the alternative operator splitting methods, described in [29], fail to resolve the dip in the s -component of the solution (see Figures 10 and 11 in [29]).

Next, we study the convergence rate of the FV-GF method with respect to the number of splitting steps. We fix the spatial mesh to 1000 uniform cells and gradually increase the number of splitting steps by powers of two. We then compute relative errors in the L^∞ and L^1 norms for each component of the solution according to the following formulae:

$$E_\infty = \frac{\|q - q^{\text{ref}}\|_\infty}{\|q^{\text{ref}}\|_\infty}, \quad E_1 = \frac{\|q - q^{\text{ref}}\|_1}{\|q^{\text{ref}}\|_1},$$

where q denotes one of the components of the splitting solution and q^{ref} denotes the same component of the reference solution. Tables 2.1–2.3 show the errors (computed at time $t = 1$ for three different grids) and the convergence rates for the s - and c -components of the solution, respectively. These results clearly demonstrate that the convergence rate starts decreasing and the error saturates when a number of splitting steps gets too large. This outcome is expected since, as it follows from the error estimates (2.12) and (2.11), the splitting step in the FV-GF method cannot be taken too small. It is also instructive to observe the convergence rates achieved with

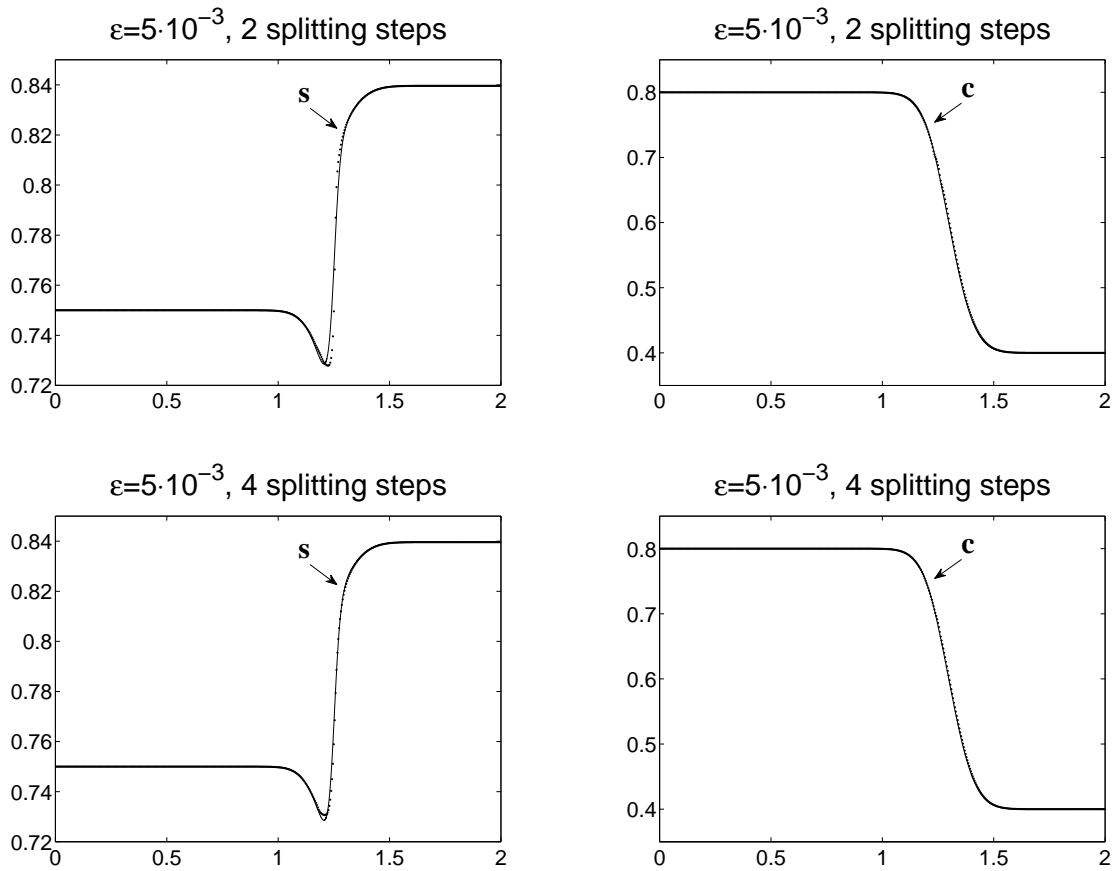


Figure 2.4: Solution of (2.16)–(2.17) computed by the FV-GF method with 2 and 4 splitting steps (dotted line). The solid line represents the reference solution.

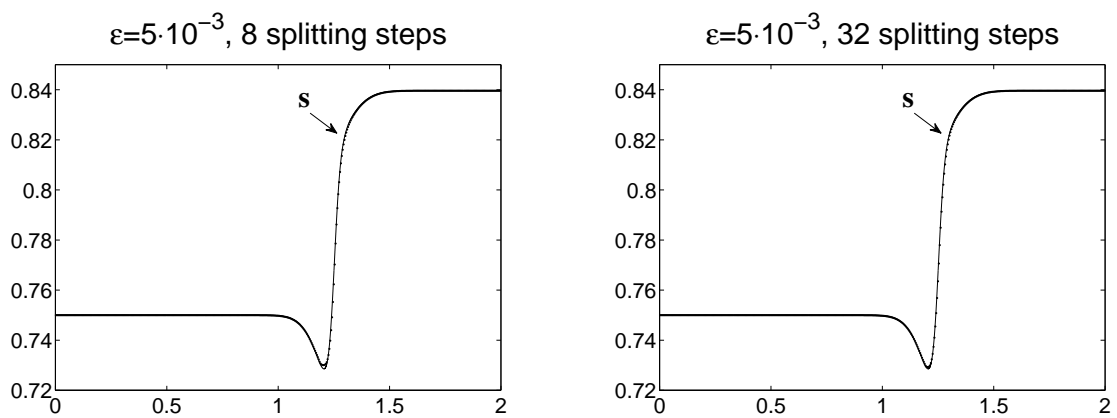


Figure 2.5: s -component of the solution of (2.16)–(2.17) computed by the FV-GF method with 8 and 32 splitting steps (dotted line). The solid line represents the reference solution.

a fixed number of splitting steps (8, 16 or 32) and gradually refined mesh (see Tables 2.4–2.6). As expected, the error rapidly decreases when we begin to refine the mesh (from $\Delta x = 1.6 \cdot 10^{-2}$ to $\Delta x = 2 \cdot 10^{-3}$), but then it saturates as the splitting error starts dominating.

Number of steps	<i>s</i> -component				<i>c</i> -component			
	L^∞ -error	Rate	L^1 -error	Rate	L^∞ -error	Rate	L^1 -error	Rate
2	1.80e-02	–	4.53e-04	–	1.63e-02	–	1.28e-03	–
4	9.95e-03	0.85	3.77e-04	0.27	1.25e-02	0.38	1.13e-03	0.17
8	7.19e-03	0.47	3.74e-04	0.01	1.16e-02	0.10	1.02e-03	0.16
16	7.02e-03	0.04	3.55e-04	0.08	1.09e-02	0.10	9.30e-04	0.13
32	7.31e-03	-0.06	3.42e-04	0.05	1.03e-02	0.08	8.86e-04	0.07
64	7.31e-03	0.00	3.35e-04	0.03	1.00e-02	0.03	8.67e-04	0.03
128	7.25e-03	0.01	3.34e-04	0.01	1.00e-02	0.00	8.61e-04	0.01
256	7.25e-03	0.00	3.34e-04	0.00	1.00e-02	0.00	8.61e-04	0.00

Table 2.1: Relative errors and convergence rates with respect to the number of splitting steps, computed on a uniform grid with $\Delta x = 8 \cdot 10^{-3}$.

Number of steps	<i>s</i> -component				<i>c</i> -component			
	L^∞ -error	Rate	L^1 -error	Rate	L^∞ -error	Rate	L^1 -error	Rate
2	2.38e-02	–	5.51e-04	–	9.18e-03	–	9.16e-04	–
4	1.01e-02	1.24	2.47e-04	1.16	5.98e-03	0.62	7.36e-04	0.32
8	5.19e-03	0.96	1.72e-04	0.52	5.75e-03	0.06	6.49e-04	0.18
16	4.00e-03	0.38	1.51e-04	0.19	5.70e-03	0.01	6.15e-04	0.08
32	3.82e-03	0.069	1.46e-04	0.05	5.65e-03	0.01	6.09e-04	0.02
64	4.79e-03	-0.33	2.12e-04	-0.53	5.11e-03	0.14	6.25e-04	-0.04
128	4.76e-03	0.01	2.11e-04	0.01	5.08e-03	0.01	6.25e-05	0.00
256	4.76e-03	0.00	2.10e-04	0.00	5.06e-03	0.00	6.25e-05	0.00

Table 2.2: Relative errors and convergence rates with respect to the number of splitting steps, computed on a uniform grid with $\Delta x = 4 \cdot 10^{-3}$.

3 The MC-GF Method

In this section, we provide a detailed description of the 1-D version of the MC-GF method, which is a recommended fast explicit operator splitting method in the case of a linear hyperbolic part.

Number of steps	s-component				c-component			
	L^∞ -error	Rate	L^1 -error	Rate	L^∞ -error	Rate	L^1 -error	Rate
2	2.56e-02	–	6.15e-04	–	5.56e-03	–	3.50e-04	–
4	7.91e-03	1.71	2.05e-04	1.59	1.89e-03	1.55	1.84e-04	0.93
8	2.28e-03	1.79	7.20e-05	1.51	1.09e-03	0.79	1.12e-04	0.72
16	6.57e-04	1.80	2.86e-05	1.33	8.21e-04	0.41	8.33e-05	0.42
32	3.63e-04	0.85	1.85e-05	0.63	6.77e-04	0.28	7.33e-05	0.18
64	3.53e-04	0.04	1.73e-05	0.10	6.06e-04	0.16	6.84e-045	0.10
128	3.52e-04	0.00	1.68e-05	0.05	5.71e-04	0.08	6.59e-05	0.05
256	3.51e-04	0.00	1.65e-05	0.02	5.55e-04	0.04	6.47e-05	0.03

Table 2.3: Relative errors and convergence rates with respect to the number of splitting steps, computed on a uniform grid with $\Delta x = 2 \cdot 10^{-3}$.

Δx	s-component				c-component			
	L^∞ -error	Rate	L^1 -error	Rate	L^∞ -error	Rate	L^1 -error	Rate
0.016	8.44e-03	–	7.36e-04	–	2.58e-02	–	3.41e-03	–
0.008	7.19e-03	0.23	3.74e-04	0.98	1.16e-02	1.15	1.02e-03	1.75
0.004	5.19e-03	0.47	1.72e-04	1.12	5.75e-03	1.01	6.49e-04	0.65
0.002	2.28e-03	1.18	7.20e-05	1.26	1.09e-03	2.39	1.12e-04	2.54
0.001	2.60e-03	-0.18	6.82e-05	0.08	6.30e-04	0.79	5.50e-05	1.02

Table 2.4: Relative errors and convergence rates computed with 8 splitting steps.

Δx	s-component				c-component			
	L^∞ -error	Rate	L^1 -error	Rate	L^∞ -error	Rate	L^1 -error	Rate
0.016	8.63e-03	–	7.40e-04	–	2.52e-02	–	3.30e-03	–
0.008	7.02e-03	0.29	3.55e-04	1.06	1.09e-02	1.21	9.30e-04	1.82
0.004	4.00e-03	0.81	1.51e-04	1.23	5.70e-03	0.93	6.15e-04	0.60
0.002	6.57e-04	2.61	2.86e-05	2.40	8.21e-04	2.80	8.33e-05	2.88
0.001	7.30e-04	-0.15	2.16e-05	0.40	3.05e-04	1.43	2.99e-05	1.48

Table 2.5: Relative errors and convergence rates computed with 16 splitting steps.

Δx	s -component				c -component			
	L^∞ -error	Rate	L^1 -error	Rate	L^∞ -error	Rate	L^1 -error	Rate
0.016	8.65e-03	–	7.40e-04	–	2.50e-02	–	3.28e-03	–
0.008	7.30e-03	0.24	3.42e-04	1.11	1.03e-02	1.28	8.86e-04	1.89
0.004	3.82e-03	0.94	1.46e-04	1.22	5.65e-03	0.86	6.09e-04	0.54
0.002	3.63e-04	3.39	1.85e-05	2.98	6.77e-04	3.06	7.33e-05	3.05
0.001	1.84e-04	0.98	7.73e-06	1.26	2.15e-04	1.65	2.11e-05	1.79

Table 2.6: Relative errors and convergence rates computed with 32 splitting steps.

To this end, we consider the following IVP:

$$q_t + u(x, t)q_x + \kappa(x, t)q = \varepsilon q_{xx}, \quad q(x, 0) = q_0(x). \quad (3.1)$$

The MC-GF method is based on the Strang operator splitting (1.9), in which the hyperbolic equation $q_t + u(x, t)q_x + \kappa(x, t)q = 0$ is numerically integrated by the method of characteristics, while the diffusion equation $q_t = \varepsilon q_{xx}$ is solved exactly using the heat kernel solution formula.

We assume that a set of characteristic points, $\{x_i(t)\}$, and the corresponding solution point values, $\{q_i(t) := q(x_i(t), t)\}$, are available at a certain time level t . The first “hyperbolic” substep of (1.9) is performed by the method of characteristics, that is, by evolving the characteristic points and the solution point values from time t to time $t + \Delta t/2$ according to the following system of ODEs:

$$\frac{dx_i(t)}{dt} = u(x_i(t), t), \quad \frac{dq_i(t)}{dt} = -\kappa(x_i(t), t)q_i(t), \quad (3.2)$$

which should be numerically integrated by an appropriate ODE solver. At the end of this substep, the solution, denoted by $\{q_i^*\}$, will be realized as a set of point values $\{q_i^* := q_i^*(t + \Delta t/2) = q(x_i^*, t + \Delta t/2)\}$ at $x_i^* := x_i(t + \Delta t/2)$. The “diffusion” substep is then carried out by evolving this intermediate solution q^* exactly according to (compare with (2.8)):

$$q^{**}(x) := q^*(x) + \int_{\mathbb{R}} G(x - \xi, \varepsilon \Delta t) (q^*(\xi) - q^*(x)) d\xi, \quad (3.3)$$

where $G(x, t)$ is the heat kernel given by (2.7). Since after the first “hyperbolic” substep only a discrete set of values $\{q_i^*\}$ is available, we apply the trapezoidal rule to formula (3.3) and end up with the new set of point values of u at the same locations $\{x_i^*\}$:

$$q_i^{**} = q_i^* + \frac{1}{2} \sum_j [G(x_i^* - x_{j+1}^*, \varepsilon \Delta t)(q_{j+1}^* - q_i^*) + G(x_i^* - x_j^*, \varepsilon \Delta t)(q_j^* - q_i^*)] (x_{j+1}^* - x_j^*). \quad (3.4)$$

Finally, we perform another “hyperbolic” substep and obtain the new set of characteristic points, $\{x_i(t + \Delta t)\}$, and the solution values there: $\{q(x_i(t + \Delta t), t + \Delta t)\}$.

This completes the description of one time step of the MC-GF method.

Remark 3.1 The 2-D generalization of the MC-GF method is rather straightforward. We would only like to comment here on the 2-D extension of the trapezoidal quadrature (3.4), which can be performed, for instance, by arranging a nonuniform set of characteristics points $\{(x_i^*, y_i^*)\}$ into the Delaunay triangulation. This determines a continuous piecewise linear approximation of the integrand in the 2-D analog of (3.3), which, in turn, can be integrated exactly: the integral over each triangle is equal to the area of the triangle multiplied by the average of the integrand values at the triangle vertices (see [11]). ■

3.1 Numerical Examples

In this section, we demonstrate the performance of the MC-GF method on a number of numerical examples. We first consider a 1-D scalar convection-diffusion equation with a linear convection flux. Then, we apply the MC-GF method in the framework of a hybrid Eulerian-Lagrangian approach to the 1-D and 2-D systems of equations modeling propagation of a passive pollutant in shallow water.

In all examples below, the ODE system (3.2) was numerically integrated using the third-order strong stability preserving (SSP) Runge-Kutta solver [22].

Example 3.1 — 1-D Linear Convection-Diffusion Equation

We first consider a simple scalar equation (3.1) with the diffusion parameter $\varepsilon = 2 \cdot 10^{-4}$, the coefficients u and κ given by

$$u(x, t) = \begin{cases} x - t, & x \leq t, \\ 0, & x > t \end{cases} \quad \text{and} \quad \kappa(x, t) = u_x(x, t) = \begin{cases} 1, & x < t, \\ 0, & x > t, \end{cases} \quad (3.5)$$

and subject to the following initial data:

$$q(x, 0) = \begin{cases} 1, & -1 \leq x \leq 1, \\ 0, & \text{otherwise.} \end{cases} \quad (3.6)$$

We numerically solve this IVP using the MC-GF method with 400 characteristic points, which are initially uniformly distributed over the interval $[-2, 2]$. In Figure 3.1 (left), the result obtained at time $t = 1$ with 4 splitting steps is compared with the numerical solution computed using a FV method applied to the convection-diffusion equation (3.5) in a straightforward manner (without splitting) over a uniform grid with $\Delta x = 1/100$. In the latter case, the semi-discrete second-order central-upwind scheme from [32] was implemented with the large stability domains explicit ODE solver DUMKA3 from [43] needed to avoid severe time step restrictions (as we discussed in the introduction, see page 4). As one can clearly see, the resolution of the moving discontinuity achieved by the MC-GF method is much sharper. This outcome is expected since the numerical diffusion present in the FV scheme oversmears the jump. If the mesh size is reduced, then the numerical diffusion decreases, and the quality of the FV solution with $\Delta x = 1/400$ becomes comparable with the one obtained in the original MC-GF calculation, see Figure 3.1 (right).

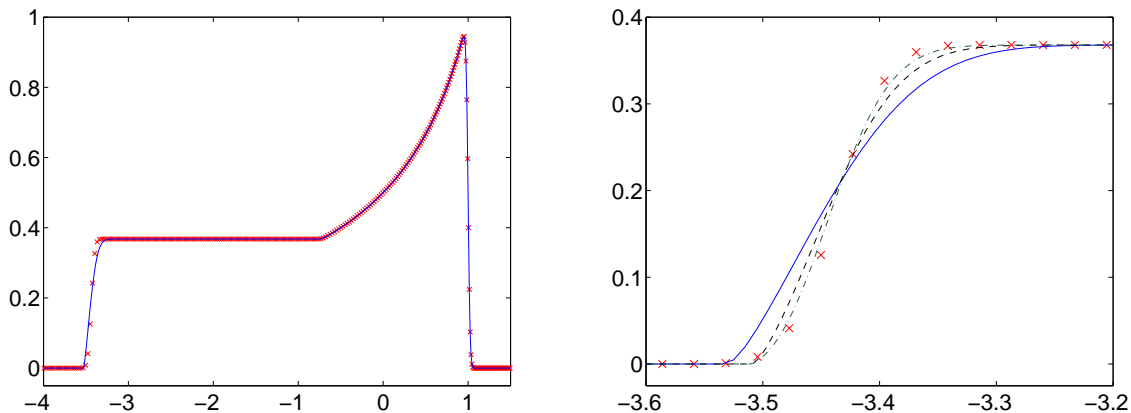


Figure 3.1: Left: Solutions of the IVP (3.1), (3.5)–(3.6) by the MC-GF method ('pluses') and the FV method (solid line). Right: Comparison of the same solutions with the FV ones computed on finer grids with $\Delta x = 1/200$ (dashed line) and $\Delta x = 1/400$ (dash-dotted line).

3.1.1 Propagation of Passive Pollutant in Shallow Water

We now consider the transport of a passive pollutant by a flow modeled by the Saint-Venant system of shallow water equations [19]. In the 1-D case, the system reads:

$$\begin{cases} h_t + (hu)_x = 0, \\ (hu)_t + \left(hu^2 + \frac{gh^2}{2} \right)_x = -ghB_x. \end{cases} \quad (3.7)$$

Here, h and u are the depth and the velocity of the water, g is the gravity constant, and the function B represents the bottom topography. The propagation of the pollutant is modeled by the convection-diffusion equation:

$$T_t + uT_x = \varepsilon T_{xx}, \quad (3.8)$$

where T is the pollutant concentration and ε is the viscosity coefficient.

This model assumes that the pollution source has been turned off and equations (3.7) and (3.8) are coupled only through the velocity u . To numerically solve the system (3.7)–(3.8) and illustrate the performance of the MC-GF method, we implement a hybrid Eulerian-Lagrangian strategy, which has been introduced in [11, 12, 15], that is, we solve (3.7) and (3.8) separately using two different methods. First, we numerically integrate the Saint-Venant system (3.7) by a FV method (we have used a semi-discrete second-order well-balanced positivity preserving central-upwind scheme from [33], but it can be replaced with any favorite FV method). Once the system (3.7) is solved for h and hu , a global approximation of u at each time level is computed by dividing a piecewise linear approximation of hu by a piecewise linear approximation of h . This gives us a velocity coefficient u in (3.8), which thus becomes a linear convection-diffusion equation, which we solve by the MC-GF method.

In the numerical experiments below, the gravitation constant was taken $g = 1$ and the viscosity coefficient $\varepsilon = 10^{-5}$. In the 2-D example, the Delaunay triangulation, needed for implementing a 2-D version of the trapezoidal quadrature (3.4), was performed using an algorithm

based on the open source mesh generation package GeomPack, available at www.geompack.org, see also www.csit.fsu.edu/~burkardt/f_src/geompack/geompack.html.

We compare the results, computed by our Eulerian-Lagrangian method, with those obtained by a “purely” Eulerian approach, in which a FV method was applied to both the Saint-Venant system (3.7) and the convection-diffusion equation (3.8). We have used the second-order central upwind scheme [32, 33], which has been applied to (3.7) and (3.8) separately, as it has been suggested in [11, 12, 15] as a way to improve the resolution of contact waves in T , achieved by the FV technique.

Example 3.2 — Propagation of a 1-D Pollution Spot

We start with the 1-D example considered in [11], in which we assume that the initial water level and the initial discharge are constant: $h(x, 0) + B(x) \equiv 1$, $h(x, 0)u(x, 0) \equiv 0.1$, the bottom topography is given by

$$B(x) = \begin{cases} 0.25(\cos(10\pi(x - 0.5)) + 1), & \text{if } 0.4 \leq x \leq 0.6, \\ 0, & \text{otherwise,} \end{cases}$$

and the initially polluted area is $[0.4, 0.5]$:

$$T(x, 0) = \begin{cases} 1, & \text{if } 0.4 \leq x \leq 0.5, \\ 0, & \text{otherwise.} \end{cases}$$

The pollution spot propagates to the right, and we numerically track its evolution. The pollutant concentrations at times $t = 0, 2$, and 4 , computed by the hybrid FV/MC-GF and the “purely” FV methods, are shown in Figure 3.2 (left), where both Δx for the central-upwind scheme and the distance between the initially uniformly distributed characteristics points is taken to be $1/200$. One can clearly see the superiority of the results obtained by the hybrid FV/MC-GF method. We then refine the mesh employed by the “purely” FV method and show the obtained solutions in Figure 3.2 (right). One can observe that the resolution achieved by the hybrid method with $\Delta x = 1/200$ is comparable with the one by the “purely” FV method with $\Delta x = 1/1600$. The difference becomes even more prominent in the 2-D case, considered in the next numerical example.

Example 3.3 — Propagation of a 2-D Pollution Spot

In this example, taken from [11], the initially polluted spot is transported with the flow over the exponentially shaped bump $B(x, y) = 0.25 \exp(-10x^2 - 5y^2)$. The 2-D version of the system (3.7)–(3.8) is solved subject to the initial conditions:

$$h(x, y, 0) + B(x, y) \equiv 1, \quad h(x, y, 0)\mathbf{u}(x, y, 0) \equiv (0.2, 0.05)^T,$$

where h is, as before, the water depth, and \mathbf{u} is the velocity vector. The initial concentration of the pollutant is:

$$T(x, y, 0) = \begin{cases} 1, & -0.75 \leq x \leq -0.25, -0.25 \leq y \leq 0.25, \\ 0, & \text{otherwise.} \end{cases}$$

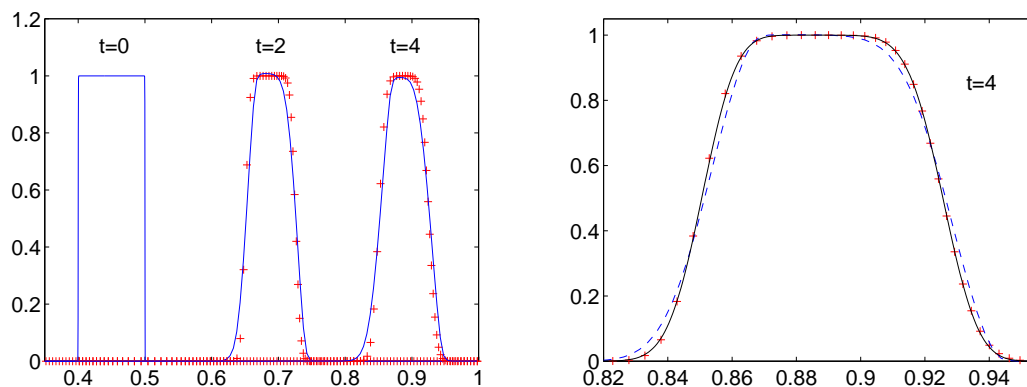


Figure 3.2: Propagation of the 1-D pollution spot by the hybrid FV/MC-GF method ('pluses') and the "purely" FV method (solid line) at different times (left figure). In the right figure: comparison of the same hybrid FV/MC-GF solution with the "purely" FV ones computed on finer grids with $\Delta x = 1/400$ (dashed line) and $\Delta x = 1/1600$ (solid line).

In Figure 3.3, we show a contour plot of the pollutant concentration T at time $t = 4$, computed by the hybrid FV/MC-GF method (left) on a uniform grid with $\Delta x = \Delta y = 1/50$ and the corresponding initial uniform distribution of the characteristic points and the "purely" FV method with $\Delta x = \Delta y = 1/200$ (right). The dashed line represents the boundary of the initially polluted domain. Like in the 1-D example, one can clearly observe a much better resolution achieved by the hybrid FV/MC-GF method even though the "purely" FV method was applied on a much finer grid.

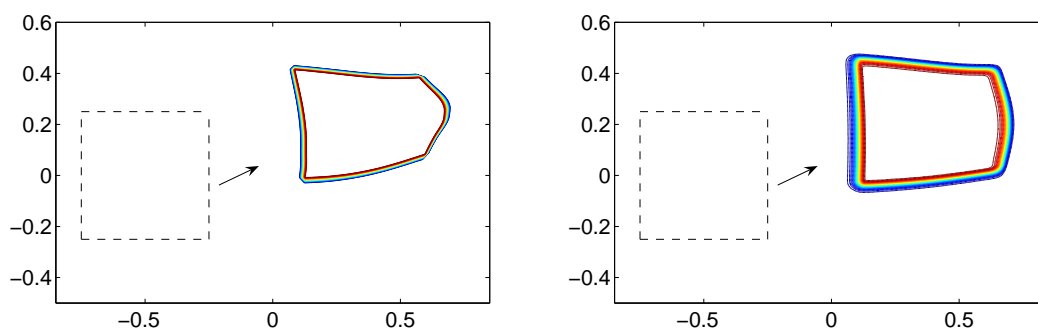


Figure 3.3: Propagation of the 2-D pollution spot by the hybrid FV/MC-GF method (left) and the "purely" FV method (right). The dashed line represents the boundary of the initially polluted domain.

4 The FD-PS Method

In this section, we present the third version of the fast explicit operator splitting method — the FD-PS method, which seems to be an optimal splitting method in the case of a viscous HJ

equation with periodic boundary conditions.

Without loss of generality, we consider the 2-D version of equation (1.2),

$$\varphi_t + H(\varphi_x, \varphi_y) = \varepsilon \Delta \varphi, \quad \varepsilon > 0, \quad (4.1)$$

with the 2π -periodic boundary conditions in both directions. The FD-PS method is based on the FD *hyperbolic* and the pseudo-spectral *parabolic* solvers implemented in the Strang splitting manner (1.9).

The “hyperbolic” substeps consist of numerical solution of the inviscid HJ equation

$$\varphi_t + H(\varphi_x, \varphi_y) = 0. \quad (4.2)$$

This can be done using any numerical method. In particular, in this paper we have implemented the semi-discrete central-upwind FD scheme from [32] (see also [7, 9, 10, 36]), according to which the point values $\{\varphi_{j,k}(t) \approx \varphi(x_j, y_k, t)\}$ are evolved in time by numerically solving the following system of time-dependent ODEs:

$$\begin{aligned} \frac{d}{dt} \varphi_{j,k}(t) = & - \frac{a_{j,k}^- b_{j,k}^- H(\varphi_x^+, \varphi_y^+) - a_{j,k}^- b_{j,k}^+ H(\varphi_x^+, \varphi_y^-) - a_{j,k}^+ b_{j,k}^- H(\varphi_x^-, \varphi_y^+) + a_{j,k}^+ b_{j,k}^+ H(\varphi_x^-, \varphi_y^-)}{(a_{j,k}^+ - a_{j,k}^-)(b_{j,k}^+ - b_{j,k}^-)} \\ & - \frac{a_{j,k}^+ a_{j,k}^-}{a_{j,k}^+ - a_{j,k}^-} (\varphi_x^+ - \varphi_x^-) - \frac{b_{j,k}^+ b_{j,k}^-}{b_{j,k}^+ - b_{j,k}^-} (\varphi_y^+ - \varphi_y^-). \end{aligned} \quad (4.3)$$

Here, $\varphi_x^\pm \approx \varphi_x(x_j \pm 0, y_k, t)$ and $\varphi_y^\pm \approx \varphi_x(x_j, y_k \pm 0, t)$ are approximations of the one-sided partial derivatives of φ at the grid point (x_j, y_k) , and $a_{j,k}^\pm, b_{j,k}^\pm$ are one-sided local speeds of propagation, which, in the case of a convex Hamiltonian, can be estimated as follows:

$$\begin{aligned} a_{j,k}^+ &:= \max_{\pm} \{H_1(\varphi_x^\pm, \varphi_y^\pm)\}_+, & a_{j,k}^- &:= \min_{\pm} \{H_1(\varphi_x^\pm, \varphi_y^\pm)\}_-, \\ b_{j,k}^+ &:= \max_{\pm} \{H_2(\varphi_x^\pm, \varphi_y^\pm)\}_+, & b_{j,k}^- &:= \min_{\pm} \{H_2(\varphi_x^\pm, \varphi_y^\pm)\}_-, \end{aligned} \quad (4.4)$$

where H_i denotes the partial derivative of the Hamiltonian H with respect to its i th arguments ($i = 1, 2$), and $(\cdot)_+ := \max(\cdot, 0)$ and $(\cdot)_- := \min(\cdot, 0)$.

In order to prevent spurious oscillations, the one-sided numerical derivatives φ_x^\pm and φ_y^\pm are to be computed using a nonlinear limiter. In the numerical example reported below, we have used the fifth-order Weighted Power-ENO reconstruction [10, 49]. Our particular choice of the ODE solver is the third-order SSP Runge-Kutta solver from [22].

Remark 4.1 The proposed FD-PS method is not tied to the central-upwind scheme (4.3)–(4.4) and can be used with any hyperbolic solver. A number of reliable high-order schemes for the inviscid HJ equation (4.2) can be found in [8, 27, 45, 46, 49, 55]. ■

The “parabolic” substep consists of numerical solution of the linear heat equation

$$\varphi_t = \varepsilon \Delta \varphi, \quad \varepsilon > 0, \quad (4.5)$$

on the square domain with the $(2\pi, 2\pi)$ -periodic boundary conditions. In this case, equation (4.5) can be exponentially accurately and efficiently solved using the pseudo-spectral method.

To do so, we first use the FFT algorithm to compute the discrete Fourier coefficients $\widehat{\varphi}_{mn}(t)$ from the available point values $\varphi_{j,k}(t)$ and approximate the solution at time t by

$$\varphi(x, y, t) \approx \sum_{m,n} \widehat{\varphi}_{mn}(t) e^{i(mx+ny)}. \quad (4.6)$$

We then plug (4.6) into (4.5) and obtain simple linear ODEs for the discrete Fourier coefficients:

$$\frac{d}{dt} \widehat{\varphi}_{mn}(t) = -\varepsilon(m^2 + n^2) \widehat{\varphi}_{mn}(t),$$

which can be easily solved exactly so that

$$\widehat{\varphi}_{mn}(t + \Delta t) = \widehat{\varphi}_{mn}(t) e^{-\varepsilon \Delta t (m^2 + n^2)}.$$

We then use the inverse FFT algorithm to obtain the point values of the solution at the new time level, $\{\varphi_{j,k}(t + \Delta t)\}$, out of the set of the discrete Fourier coefficients, $\{\widehat{\varphi}_{mn}(t + \Delta t)\}$.

Remark 4.2 As in the previously presented (see §2 and §3) versions of the fast explicit operator splitting method, the pseudo-spectral parabolic solver of the FD-PS method can be used with an arbitrarily large splitting time step Δt . Therefore, in the convection-dominated regime, that is, when ε is very small, a highly accurate numerical solution of the viscous HJ equation (4.1) can be obtained with only few splitting steps. \blacksquare

At the end of this section, we test the proposed FD-PS method on the following numerical example.

Example 4.1 — 2-D Incompressible Navier-Stokes Equation

We consider the incompressible NS equation

$$\mathbf{u}_t + (\mathbf{u} \cdot \nabla) \mathbf{u} + \nabla p = \varepsilon \Delta \mathbf{u}, \quad (4.7)$$

where p denotes the pressure and $\mathbf{u} = (u, v)^T$ is the divergence-free velocity field, satisfying $u_x + v_y = 0$. It is well-known that in the 2-D case, the NS equation (4.7) admits an equivalent vorticity formulation, which can be written in the transport form:

$$\omega_t + u\omega_x + v\omega_y = \varepsilon \Delta \omega, \quad (4.8)$$

where ω is the vorticity, $\omega := v_x - u_y$. Equation (4.8) can be viewed as a 2-D viscous HJ equation

$$\omega_t + H(\omega_x, \omega_y) = \varepsilon \Delta \omega, \quad (4.9)$$

with a global Hamiltonian $H(\omega_x, \omega_y) = u\omega_x + v\omega_y$.

We apply the FD-PS method to the vorticity equation (4.9). Choosing the one-sided local speeds, $a_{j,k}^\pm$ and $b_{j,k}^\pm$, as

$$a_{j,k}^\pm := (u_{j,k})_\pm, \quad b_{j,k}^\pm := (v_{j,k})_\pm, \quad (4.10)$$

we obtain the following simpler form of the central-upwind scheme (4.3)–(4.4):

$$\begin{aligned} \frac{d}{dt}\omega_{j,k}(t) = & -\frac{a_{j,k}^- b_{j,k}^- (u_{j,k}\omega_x^+ + v_{j,k}\omega_y^+) - a_{j,k}^- b_{j,k}^+ (u_{j,k}\omega_x^+ + v_{j,k}\omega_y^-)}{(a_{j,k}^+ - a_{j,k}^-)(b_{j,k}^+ - b_{j,k}^-)} \\ & + \frac{a_{j,k}^+ b_{j,k}^- (u_{j,k}\omega_x^- + v_{j,k}\omega_y^+) - a_{j,k}^+ b_{j,k}^+ (u_{j,k}\omega_x^- + v_{j,k}\omega_y^-)}{(a_{j,k}^+ - a_{j,k}^-)(b_{j,k}^+ - b_{j,k}^-)}, \end{aligned} \quad (4.11)$$

where the one-sided numerical derivatives $\omega_x^\pm \approx \omega_x(x_j \pm 0, y_k, t)$ and $\omega_y^\pm \approx \omega_y(x_j, y_k \pm 0, t)$. We compute these derivatives using the fifth-order Weighted Power-ENO reconstruction [10, 49].

Since the Hamiltonian is global, the implementation of the scheme (4.10)–(4.11) requires the velocities $\{u_{j,k}, v_{j,k}\}$ to be recovered from the known values of the vorticity $\{\omega_{j,k}\}$ at each time level. This can be done with the help of the stream function ψ , such that $u = \psi_y$, $v = -\psi_x$, and $\Delta\psi = -\omega$. To solve this Poisson equation, we use the FFT based pseudo-spectral method, and then compute the velocities via the fourth-order finite differences of the stream function:

$$u_{j,k} = \frac{-\psi_{j,k+2} + 8\psi_{j,k+1} - 8\psi_{j,k-1} + \psi_{j,k-2}}{12\Delta y}, \quad v_{j,k} = \frac{\psi_{j+2,k} - 8\psi_{j+1,k} + 8\psi_{j-1,k} - \psi_{j-2,k}}{12\Delta x}.$$

We apply the resulting method to the double shear-layer model problem, proposed in [5], see also [6, 32]. The initial data are

$$u(x, y, 0) = \begin{cases} \tanh(\frac{1}{\rho}(y - \pi/2)), & y \leq \pi, \\ \tanh(\frac{1}{\rho}(3\pi/2 - y)), & y > \pi, \end{cases} \quad v(x, y, 0) = \delta \cdot \sin x.$$

We take $\rho = \pi/15$, $\delta = 5 \cdot 10^{-2}$, the viscosity coefficient $\varepsilon = 5 \cdot 10^{-4}$, the final time $t = 10$, and the number of splitting steps 10.

The vorticities, computed with the FD-PS method on the 64×64 and 128×128 grids are shown in Figure 4.1 (a)–(b). These results are compared with the unsplit results, obtained using the same FD scheme for the convection part and the fourth-order central difference approximation of the Laplace operator, see Figure 4.1 (c)–(d), and with the numerical solution of the incompressible Euler equations, see Figure 4.1 (e)–(f). As one may observe, the FD-PS method achieves a super resolution without producing any spurious oscillations typically appearing near the stagnation point in the inviscid calculations, see Figure 4.1 (e)–(f). We then perform the same computations on the finer 256×256 and 512×512 grids. The obtained results are presented in Figure 4.2. Once again, we see that the FD-PS method has a sufficient amount of (physical) viscosity to suppress stagnation point oscillations, even though the size of the splitting step remains very large ($\Delta t = 1$).

5 Conclusion

In this paper, we have provided a review of fast explicit operator splitting methods for convection-diffusion equations and related problems. The methods we have presented are based on Strang operator splitting. The main advantage of the discussed methods is their efficiency, achieved by

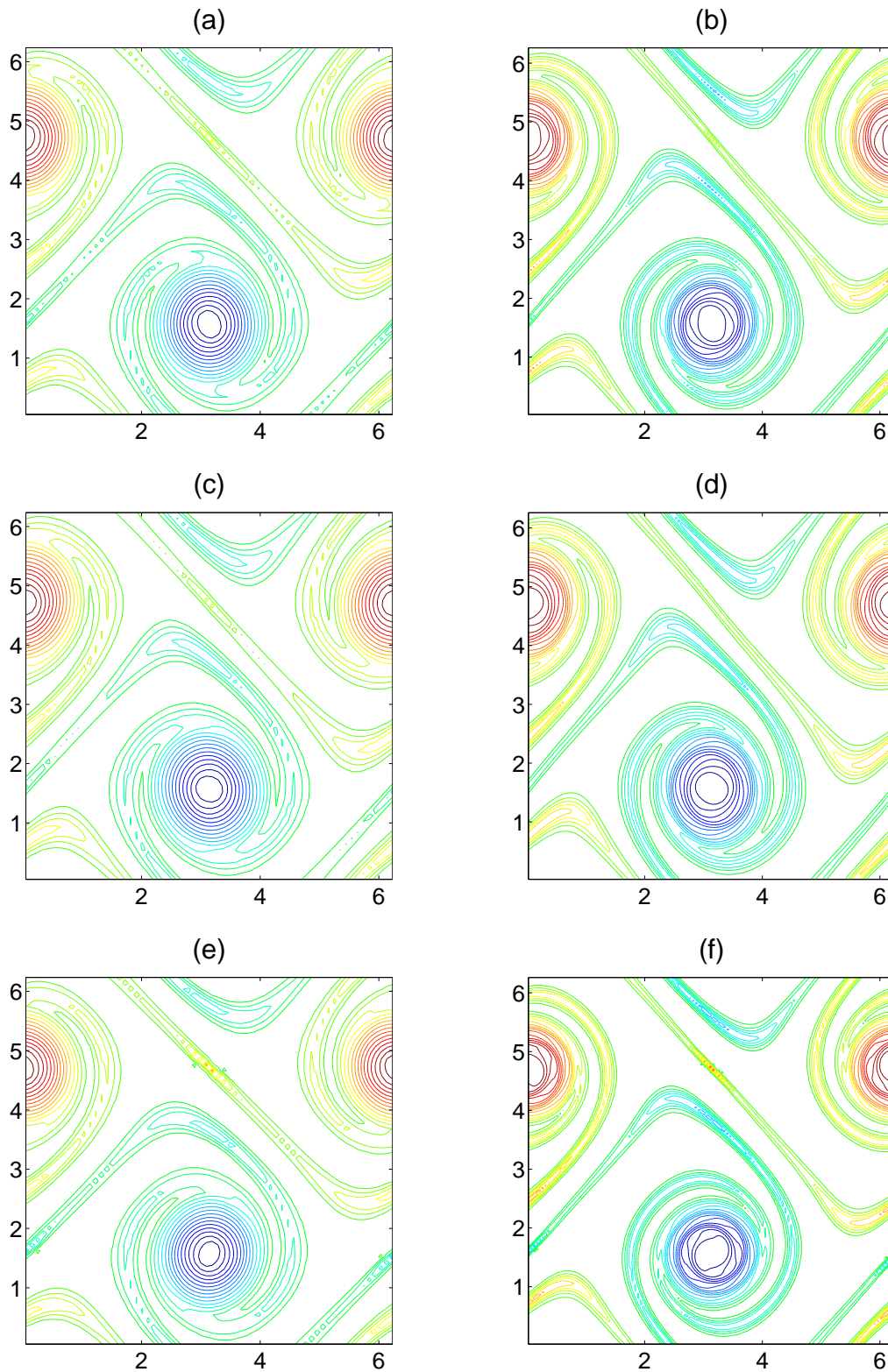


Figure 4.1: The vorticities computed by the FD-PS, (a,b), and the unsplit FD, (c,d), methods on the 64×64 , (a,c), and 128×128 , (b,d), grids. The corresponding inviscid solution is shown in (e) and (f).

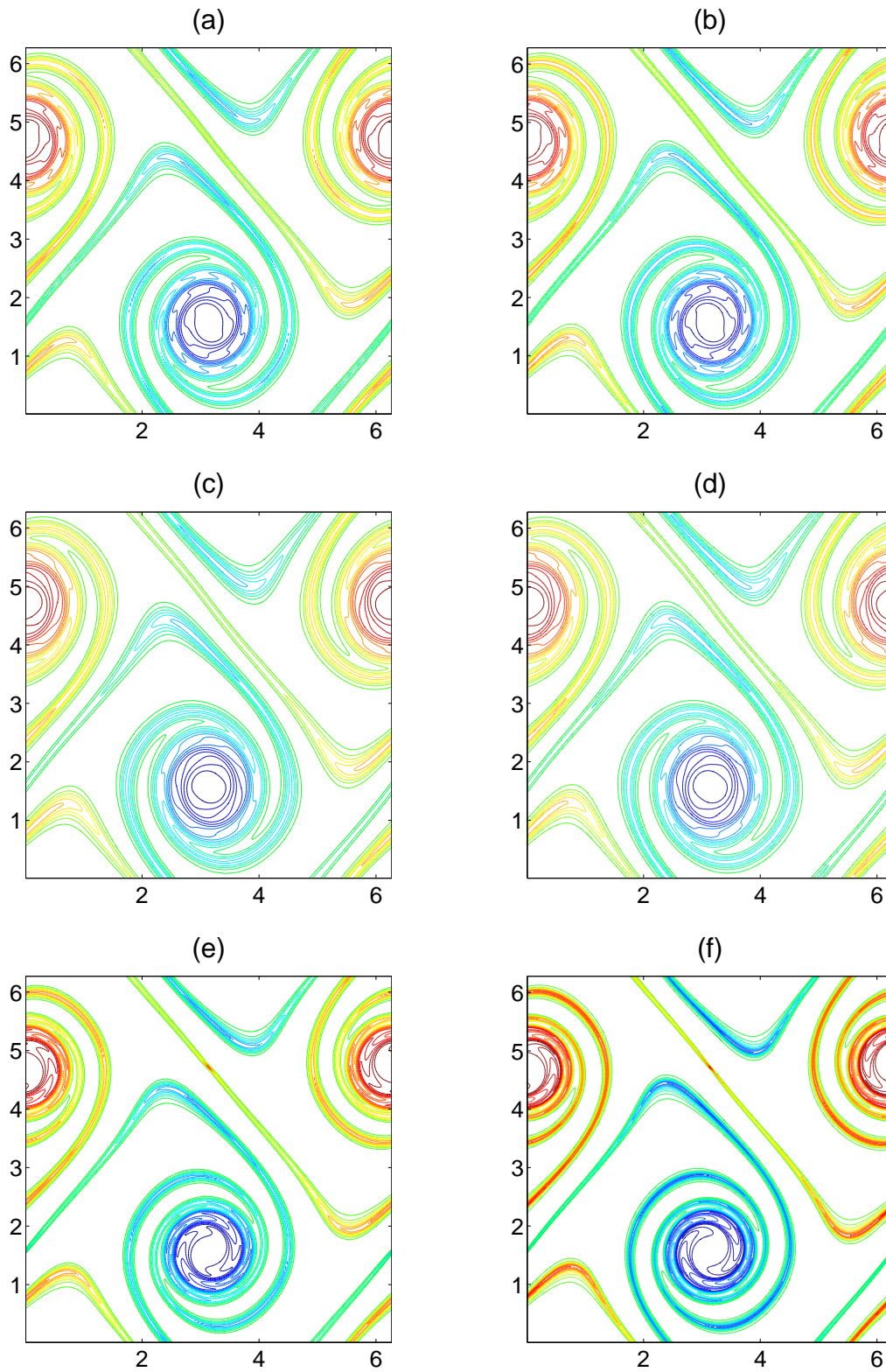


Figure 4.2: The vorticities computed by the FD-PS, (a,b), and the unsplit FD, (c,d), methods on the 256×256 , (a,c), and 512×512 , (b,d), grids. The corresponding inviscid solution is shown in (e) and (f).

the implementation of the exact parabolic solver, and a high resolution, achieved by a careful selection of the hyperbolic solvers that provide the best results for each problem at hand.

We have described three versions of the fast explicit operator splitting method, two of which (the FV-GF and the MC-GF ones) have been already introduced in [13,14] and [11], respectively, while the third one, the FD-PS method, is new. In every concrete situation, the selection of a particular version of the fast explicit operator splitting method is based on the nature of the corresponding “pure” hyperbolic problem. When the hyperbolic problem is a nonlinear system of conservation laws, then a finite-volume scheme, used in the FV-GF method, is the the best shock-capturing option. When the “pure” hyperbolic problem is a linear transport equation, then a nondiffusive method of characteristics, implemented in the MC-GF version of the fast explicit operator splitting method, seems to give the best resolution. Finally, if the incompressible Navier-Stokes equation is being numerically solved, then a high-order finite-difference scheme, used in the FD-PS method, seems to be preferable.

A superb performance of each of the three versions of the fast explicit operator splitting method has been demonstrated on a number of 1-D and 2-D numerical examples.

Acknowledgment: A. Chertock was supported in part by the NSF Grants DMS-0410023 and DMS-0712898. A. Kurganov was supported in part by the NSF Grant DMS-0610430.

References

- [1] A. ABDULLE, *Fourth order Chebyshev methods with recurrence relation*, SIAM J. Sci. Comput., 23 (2002), pp. 2041–2054 (electronic).
- [2] A. ABDULLE AND A.A. MEDOVIKOV, *Second order Chebyshev methods based on orthogonal polynomials*, Numer. Math., 90 (2001), pp. 1–18.
- [3] U.M ASCHER AND L.R. PETZOLD, *Computer methods for ordinary differential equations and differential-algebraic equations*, Society for Industrial and Applied Mathematics (SIAM), Philadelphia, PA, 1998.
- [4] U.M. ASCHER, S.J. RUUTH, AND R.J. SPITERI, *Implicit-explicit Runge-Kutta methods for time-dependent partial differential equations*, Appl. Numer. Math., 25 (1997), pp. 151–167. Special issue on time integration (Amsterdam, 1996).
- [5] J.B. BELL, P. COLELLA, AND H.M. GLAZ, *A second-order projection method for the incompressible Navier-Stokes equations*, J. Comput. Phys., 85 (1989), pp. 257–283.
- [6] D.L. BROWN AND M.L. MINION, *Performance of under-resolved two-dimensional incompressible flow simulations*, J. Comput. Phys., 122 (1995), pp. 165–183.
- [7] S. BRYSON, A. KURGANOV, D. LEVY, AND G. PETROVA, *Semi-discrete central-upwind schemes with reduced dissipation for Hamilton-Jacobi equations*, IMA J. Numer. Anal., 25 (2005), pp. 113–138.
- [8] S. BRYSON AND D. LEVY, *High-order central WENO schemes for multidimensional Hamilton-Jacobi equations*, SIAM J. Numer. Anal., 41 (2003), pp. 1339–1369 (electronic).

- [9] S. BRYSON AND D. LEVY, *High-order semi-discrete central-upwind schemes for multi-dimensional Hamilton-Jacobi equations*, J. Comput. Phys., 189 (2003), pp. 63–87.
- [10] S. BRYSON AND D. LEVY, *Mapped WENO and weighted power ENO reconstructions in semi-discrete central schemes for Hamilton-Jacobi equations*, Appl. Numer. Math., 56 (2006), pp. 1211–1224.
- [11] A. CHERTOCK, E. KASHDAN, AND A. KURGANOV, *Propagation of diffusing pollutant by a hybrid Eulerian-Lagrangian method*, in Hyperbolic problems: theory, numerics, applications (Lyon 2006), Sylvie Benzoni-Gavage and Denis Serre, eds., Springer, 2008, pp. 371–380.
- [12] A. CHERTOCK AND A. KURGANOV, *On a hybrid finite-volume particle method*, M2AN Math. Model. Numer. Anal, 38 (2004), pp. 1071–1091.
- [13] A. CHERTOCK, A. KURGANOV, AND G. PETROVA, *Fast explicit operator splitting method for convection-diffusion equations*, Internat. J. Numer. Meth. Fluids. In press.
- [14] A. CHERTOCK, A. KURGANOV, AND G. PETROVA, *Fast explicit operator splitting method. Application to the polymer system*, in Finite Volumes for Complex Applications IV, 2005, pp. 63–72.
- [15] A. CHERTOCK, A. KURGANOV, AND G. PETROVA, *Finite-volume-particle methods for models of transport of pollutant in shallow water*, J. Sci. Comput., 27 (2006), pp. 189–199.
- [16] A.J. CHORIN, *Numerical study of slightly viscous flow*, J. Fluid Mech., 57 (1973), pp. 785–796.
- [17] B. COCKBURN, C. JOHNSON, C.-W. SHU, AND E. TADMOR, *Advanced numerical approximation of nonlinear hyperbolic equations*, in CIME Lecture Notes, A. Quarteroni, ed., vol. 1697 of Lecture Notes in Mathematics, Springer-Verlag, 1997.
- [18] G.-H. COTTET AND P.D. KOUMOUTSAKOS, *Vortex methods*, Cambridge University Press, Cambridge, 2000.
- [19] A.J.C. DE SAINT-VENANT, *Théorie du mouvement non-permanent des eaux, avec application aux crues des rivières et à l'introduction des marées dans leur lit.*, C.R. Acad. Sci. Paris, 73 (1871), pp. 147–154.
- [20] E. GODLEWSKI AND P.-A. RAVIART, *Numerical approximation of hyperbolic systems of conservation laws*, vol. 118 of Applied Mathematical Sciences, Springer-Verlag, New York, 1996.
- [21] D. GOTTLIEB AND S.A. ORSZAG, *Numerical analysis of spectral methods: theory and applications*, Society for Industrial and Applied Mathematics, Philadelphia, Pa., 1977. CBMS-NSF Regional Conference Series in Applied Mathematics, No. 26.
- [22] S. GOTTLIEB, C.-W. SHU, AND E. TADMOR, *High order time discretization methods with the strong stability property*, SIAM Rev., 43 (2001), pp. 89–112.

- [23] E. HAIRER AND G. WANNER, *Solving ordinary differential equations. II*, vol. 14 of Springer Series in Computational Mathematics, Springer-Verlag, Berlin, second ed., 1996. Stiff and differential-algebraic problems.
- [24] V. HAUGSE, K.H. KARLSEN, K.-A. LIE, AND J.R. NATVIG, *Numerical solution of the polymer system by front tracking*, Transp. Porous Media, 44 (2001), pp. 63–83.
- [25] J.S HESTHAVEN, S. GOTTLIEB, AND D. GOTTLIEB, *Spectral methods for time-dependent problems*, vol. 21 of Cambridge Monographs on Applied and Computational Mathematics, Cambridge University Press, Cambridge, 2007.
- [26] W. HUNSDORFER AND J. VERWER, *Numerical solution of time-dependent advection-diffusion-reaction equations*, vol. 33 of Springer Series in Computational Mathematics, Springer-Verlag, Berlin, 2003.
- [27] G.-S. JIANG AND D. PENG, *Weighted ENO schemes for Hamilton-Jacobi equations*, SIAM J. Sci. Comput., 21 (2000), pp. 2126–2143 (electronic).
- [28] T. JOHANSEN AND R. WINTHER, *The solution of the Riemann problem for a hyperbolic system of conservation laws modeling polymer flooding*, SIAM J. Math. Anal., 19 (1988), pp. 541–566.
- [29] K.H. KARLSEN, K.-A. LIE, J.R. NATVIG, H.F. NORDHAUG, AND H.K. DAHLE, *Operator splitting methods for systems of convection-diffusion equations: nonlinear error mechanisms and correction strategies*, J. Comput. Phys., 173 (2001), pp. 636–663.
- [30] D. KRÖNER, *Numerical schemes for conservation laws*, Wiley-Teubner Series Advances in Numerical Mathematics, John Wiley & Sons Ltd., Chichester, 1997.
- [31] A. KURGANOV AND C.-T. LIN, *On the reduction of numerical dissipation in central-upwind schemes*, Commun. Comput. Phys., 2 (2007), pp. 141–163.
- [32] A. KURGANOV, S. NOELLE, AND G. PETROVA, *Semi-discrete central-upwind scheme for hyperbolic conservation laws and Hamilton-Jacobi equations*, SIAM J. Sci. Comput., 21 (2001), pp. 707–740.
- [33] A. KURGANOV AND G. PETROVA, *A second-order well-balanced positivity preserving central-upwind scheme for the Saint-Venant system*, Commun. Math. Sci., 5 (2007), pp. 133–160.
- [34] A. KURGANOV, G. PETROVA, AND B. POPOV, *Adaptive semi-discrete central-upwind schemes for nonconvex hyperbolic conservation laws*, SIAM J. Sci. Comput., 29 (2007), pp. 2381–2401.
- [35] A. KURGANOV AND E. TADMOR, *New high resolution central schemes for nonlinear conservation laws and convection-diffusion equations*, J. Comput. Phys., 160 (2000), pp. 241–282.
- [36] A. KURGANOV AND E. TADMOR, *New high-resolution semi-discrete central scheme for Hamilton-Jacobi equations*, J. Comput. Phys., 160 (2000), pp. 720–742.

- [37] J. LEE AND B. FORNBERG, *A split step approach for the 3-D Maxwell's equations*, J. Comput. Appl. Math., 158 (2003), pp. 485–505.
- [38] R.J. LEVEQUE, *Finite volume methods for hyperbolic problems*, Cambridge Texts in Applied Mathematics, Cambridge University Press, Cambridge, 2002.
- [39] R. LEVEQUE, *Finite-difference methods for ordinary and partial differential equations, steady state and time dependent problems*, Society for Industrial and Applied Mathematics (SIAM), Philadelphia, PA, 2007.
- [40] K.-A. LIE AND S. NOELLE, *On the artificial compression method for second-order nonoscillatory central difference schemes for systems of conservation laws*, SIAM J. Sci. Comput., 24 (2003), pp. 1157–1174.
- [41] G.I MARCHUK, *Metody rasshchepleniya*, (Russian) [Splitting Methods] “Nauka”, Moscow, 1988.
- [42] G.I MARCHUK, *Splitting and alternating direction methods*, in Handbook of numerical analysis, Vol. I, Handb. Numer. Anal., I, North-Holland, Amsterdam, 1990, pp. 197–462.
- [43] A.A. MEDOVIKOV, *High order explicit methods for parabolic equations*, BIT, 38 (1998), pp. 372–390.
- [44] H. NESSYAHU AND E. TADMOR, *Nonoscillatory central differencing for hyperbolic conservation laws*, J. Comput. Phys., 87 (1990), pp. 408–463.
- [45] S. OSHER AND C.-W. SHU, *High-order essentially nonoscillatory schemes for Hamilton-Jacobi equations*, SIAM J. Numer. Anal., 28 (1991), pp. 907–922.
- [46] J. QIU AND C.-W. SHU, *Hermite WENO schemes for Hamilton-Jacobi equations*, J. Comput. Phys., 204 (2005), pp. 82–99.
- [47] P.-A. RAVIART, *An analysis of particle methods*, in Numerical methods in fluid dynamics (Como, 1983), vol. 1127 of Lecture Notes in Math., Springer, Berlin, 1985, pp. 243–324.
- [48] N.H. RISEBRO AND A. TVEITO, *Front tracking applied to a non-strictly hyperbolic system of conservation laws*, SIAM J. Sci. Statist. Comput., 12 (1991), pp. 1401–1419.
- [49] S. SERNA AND J. QIAN, *Fifth-order weighted power-ENO schemes for Hamilton-Jacobi equations*, J. Sci. Comput., 29 (2006), pp. 57–81.
- [50] J. SHEN AND T. TANG, *Spectral and high-order methods with applications*, Science Press, Beijing, 2006.
- [51] G. STRANG, *On the construction and comparison of difference schemes*, SIAM J. Numer. Anal., 5 (1968), pp. 506–517.
- [52] M. SUZUKI, *General theory of fractal path integrals with applications to many-body theories and statistical physics*, J. Math. Phys., 32 (1991), pp. 400–407.

- [53] P.K. SWEBY, *High resolution schemes using flux limiters for hyperbolic conservation laws*, SIAM J. Numer. Anal., 21 (1984), pp. 995–1011.
- [54] A. TVEITO, *Convergence and stability of the Lax-Friedrichs scheme for a nonlinear parabolic polymer flooding problem*, Adv. in Appl. Math., 11 (1990), pp. 220–246.
- [55] Z. XU AND C.-W. SHU, *Anti-diffusive high order WENO schemes for Hamilton-Jacobi equations*, Methods Appl. Anal., 12 (2005), pp. 169–190.
- [56] H. YOSHIDA, *Construction of higher order symplectic integrators*, Phys. Lett. A, 150 (1990), pp. 262–268.